

PNAS

www.pnas.org

Supplementary Information for

Chondrules Reveal Large-Scale Outward Transport of Inner Solar System Materials in the Protoplanetary Disk

Curtis D. Williams^{1,*}, Matthew E. Sanborn¹, Céline Defouilloy^{2,†}, Qing-zhu Yin^{1,*}, Noriko T. Kita², Denton S. Ebel³, Akane Yamakawa^{1,#}, Katsuyuki Yamashita³

Paste corresponding author name here

Email: cdwill@ucdavis.edu, qyin@ucdavis.edu, noriko@geology.wisc.edu

This PDF file includes:

Supplementary text
Figures S1 to S5
Datasets S1 to S6
SI References

Supplementary Information Text

Chondrule texture and mineral chemistry

Nine out of 10 chondrules in Allende are ferromagnesian chondrules, consisting of 3 barred olivine (BO), 4 porphyritic olivine-pyroxene (POP), and 2 porphyritic olivine (PO) chondrules (Fig. S1). Porphyritic chondrules show coarse olivine and pyroxene phenocrysts up to 200 μm in size. Widths of olivine bars in BO chondrules are variable within and among chondrules from 25 to 150 μm . One of the BO chondrules, ALL-C1 (4284-A, Fig. S1A) contains coarse ($\sim 300 \mu\text{m}$) chromium-rich spinel, which enclose olivine bars. FeO-poor olivine grains in Allende chondrules sometime show FeO-enrichment towards to the grain boundary, which might be caused by Fe-Mg diffusion during the thermal metamorphism on the parent body. Mesostasis of these chondrules show fine structures with devitrified feldspathic mesostasis and Ca-pyroxene micro-crystallites. Olivine and pyroxene phenocrysts are rimmed with $\sim 20 \mu\text{m}$ thick high-Ca pyroxene, which are either quench overgrowths, or overgrowths due to thermal metamorphism. A tenth chondrule, ALL-C6 (4327-8, Fig. S1), is an Al-rich chondrule containing olivine, low-Ca and high-Ca pyroxene, and abundant Ca-rich plagioclase. The grain sizes of olivine in this chondrule are smaller ($< 20 \mu\text{m}$ in size) compared to the other Allende chondrules. In Karoonda, seven out of nine chondrules are PO, while the remaining two show BO texture (Fig. S2). Mesostasis areas are significantly recrystallized to high-Ca pyroxene and feldspars. Chondrule KR-C3, 22 (PO) contains 50-100 μm sized hercynite-rich spinel grains set in feldspar-rich mesostasis, which might be recrystallized from Al-rich mesostasis. The textures of individual chondrules and constituent mineral phases are more evident from composite elemental maps in Figs. 3-4.

Representative electron microprobe analyses of olivine and pyroxene for both Allende and Karoonda chondrules are listed in Dataset S5. The Mg# of olivine and pyroxene in Allende range from 83.2 to 99.5 and from 95.0 to 97.3, respectively. Three chondrules show lower Mg# (≤ 90) in the range of FeO-rich (or type II) chondrules, but all with BO textures. Other chondrules show Mg# > 90 , indicating they are FeO-poor (type I) chondrules. Olivine Mg# in each chondrule are somewhat variable, especially for those with higher Fo contents (> 90), due to Fe-Mg diffusion from parent body metamorphism. In type I POP chondrules, the Mg# of low-Ca pyroxene grains show a narrower and higher values than co-existing olivine. Thus, we estimated the original Mg# of each Allende chondrule prior to thermal metamorphism using either the maximum Fo contents of olivine or the maximum Mg# of low-Ca pyroxene, whichever was the highest (see Dataset S5). In contrast, olivine in Karoonda chondrules are equilibrated and show a narrow range of Mg# from 65.4 to 69.8. There are no distinctions between BO and PO and all chondrules show very similar silicate compositions, while many of them preserved their original porphyritic or barred olivine textures. Since Karoonda is an equilibrated CK chondrite (CK4), we rarely see pyroxene phenocrysts in chondrules, which might have been recrystallized to FeO-rich olivine (77). Limited electron probe analyses of low Ca pyroxene in Karoonda show small variabilities in their endmember enstatite, wollastonite, and ferrosilite compositions (see Dataset S5).

In the present study, textural types of the 10 Allende chondrules appear to be associated with distinct ranges of olivine and pyroxene Mg#: the highest Mg# = 99.5 are observed in PO, intermediate Mg# around 94-97 in POP and the Al-rich chondrule, while BO show lower Mg#, ranging from 83 to 90. In contrast, more than 50 chondrules in other, more-pristine CV3 chondrites, Kaba (CV_{OXB}) and NWA 8613 (CV_{red}), are dominated by those with highest Mg# (≥ 99) and do not show any correlation between textures and Mg# (14, 16). Given the limited number of chondrules selected, this may be coincidental. However, finding three FeO-rich BO chondrules out of 10 Allende chondrules is unexpected as the abundance of FeO-rich (Mg# < 90) chondrules in CV chondrites is only 5% of their whole chondrule populations (78).

Results of SIMS oxygen isotope analyses

A total of 152 unknown analyses were obtained from 19 chondrules. For each chondrule, eight olivine or pyroxene grains were analyzed for their oxygen three-isotope ratios. In ALL-C11, we obtained 9 analyses as one analysis was significantly ^{16}O -rich. In KR-C4, we discard one analysis that hit spinel by mistake. Four analysis of SCOL standard grains in the same mounts were analyzed as running standards every ~ 16 unknown measurements. A total of eight SCOL standard analyses before and after unknown analyses were used to estimate external reproducibility of $\delta^{18}\text{O}$, $\delta^{17}\text{O}$, $\Delta^{17}\text{O}$ values. Endmember Fo, En, Wo, and Fs, in olivine and

pyroxene, respectively, which were obtained from SEM-EDS analyses, were used to estimate instrumental biases of each analysis. The results of individual analyses are listed in Dataset S3. For seven out of ten Allende chondrules, multiple spot analyses of a single chondrule show indistinguishable $\Delta^{17}\text{O}$ values within 3SD of external reproducibility estimated from 8 bracket analyses of SCOL. In two chondrules, ALL-C5 (4327-6) and ALL-C11 (4308-A), all analyses are indistinguishable, except for one olivine grain in each, that is significantly ^{16}O -rich, indicating that these are relict olivine grains. The Al-rich chondrule (ALL-C6, 4327-8) shows significantly heterogeneous oxygen isotope ratios with a range of $\delta^{18}\text{O}$ and $\delta^{17}\text{O}$ values from -40‰ to -15‰ , suggesting that the chondrule contains significant amounts of relict olivine grains and that estimation of a representative oxygen isotope ratio of the chondrule is not possible. Thus, excluding ALL-C6 (4327-8), the mean $\delta^{18}\text{O}$, $\delta^{17}\text{O}$, $\Delta^{17}\text{O}$ values are calculated as the average of all analyses excluding relict olivine grains (see Datasets S3-S4). These averages represent oxygen isotope ratios of chondrule melts when these chondrules formed (e.g., **13-14, 16, 44**). The uncertainties quoted for mean values are propagated from analytical reproducibility of running standard and variabilities among multiple analyses within single chondrules, according to the protocols described in (**14, 16**).

Fig. S1. Back-scattered electron images of Allende chondrules. Textures of ferromagnesian chondrules are indicated as barred olivine (BO), porphyritic olivine (PO), and porphyritic olivine-pyroxene (POP). ALL-C6 is an Al-rich chondrule that contain abundant anorthite-rich plagioclase.

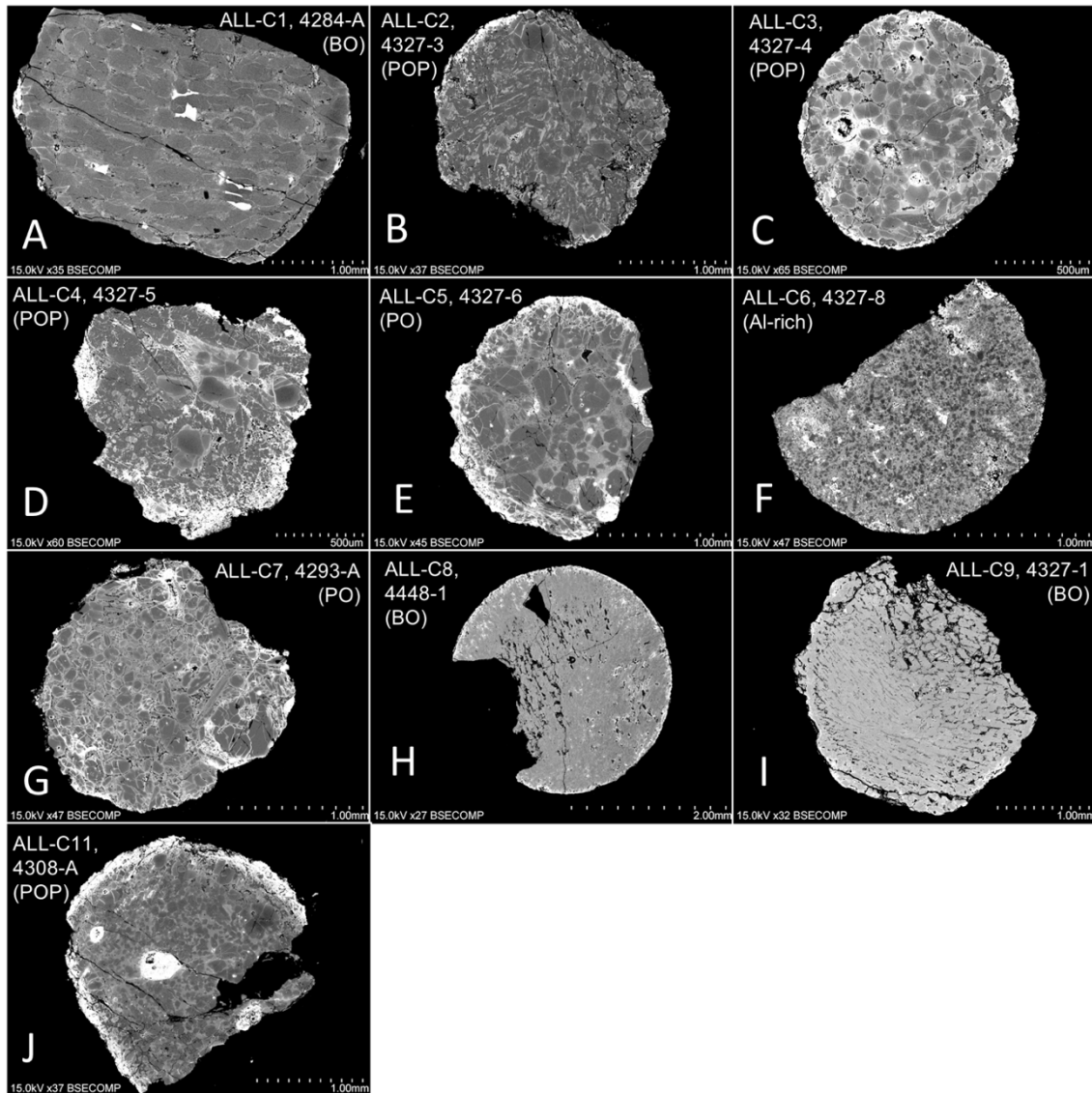


Fig. S2. Back-scattered electron images of Karoonda chondrules. Notations as in Fig. S1.

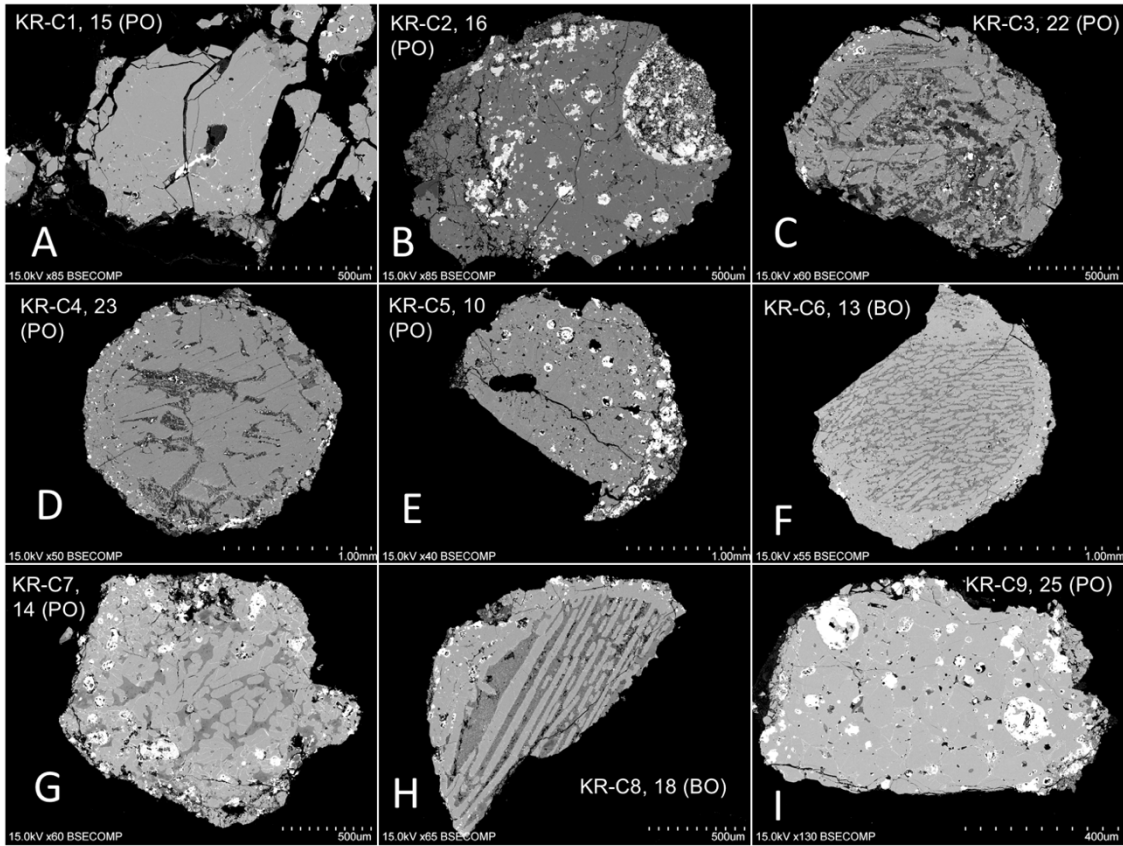


Fig. S3. Combined X-ray elemental maps of Allende chondrules. Maps with Mg (red)- Ca (green)- Al (blue) in A, G, H, and J reveal olivine as bright red, low-Ca pyroxene as darker red, high Ca-pyroxene as green, feldspathic glass and plagioclase as darker blue. In ALL-C1 (A), Cr-rich spinel appears as darker blue. Maps with Si-Ca-Al in B, C, and F show olivine as darker red, low-Ca pyroxene as brighter red, high-Ca pyroxene as yellow, and feldspathic glass and plagioclase as purple to grey. Maps with Si-Ca-Fe in D and E show olivine as darker red, low-Ca pyroxene as brighter red, high-Ca pyroxene as yellow. The map for BO chondrule ALL-C9 (I) with Mg-Si-Al=R-G-B shows olivine bars as yellow and mesostasis as green.

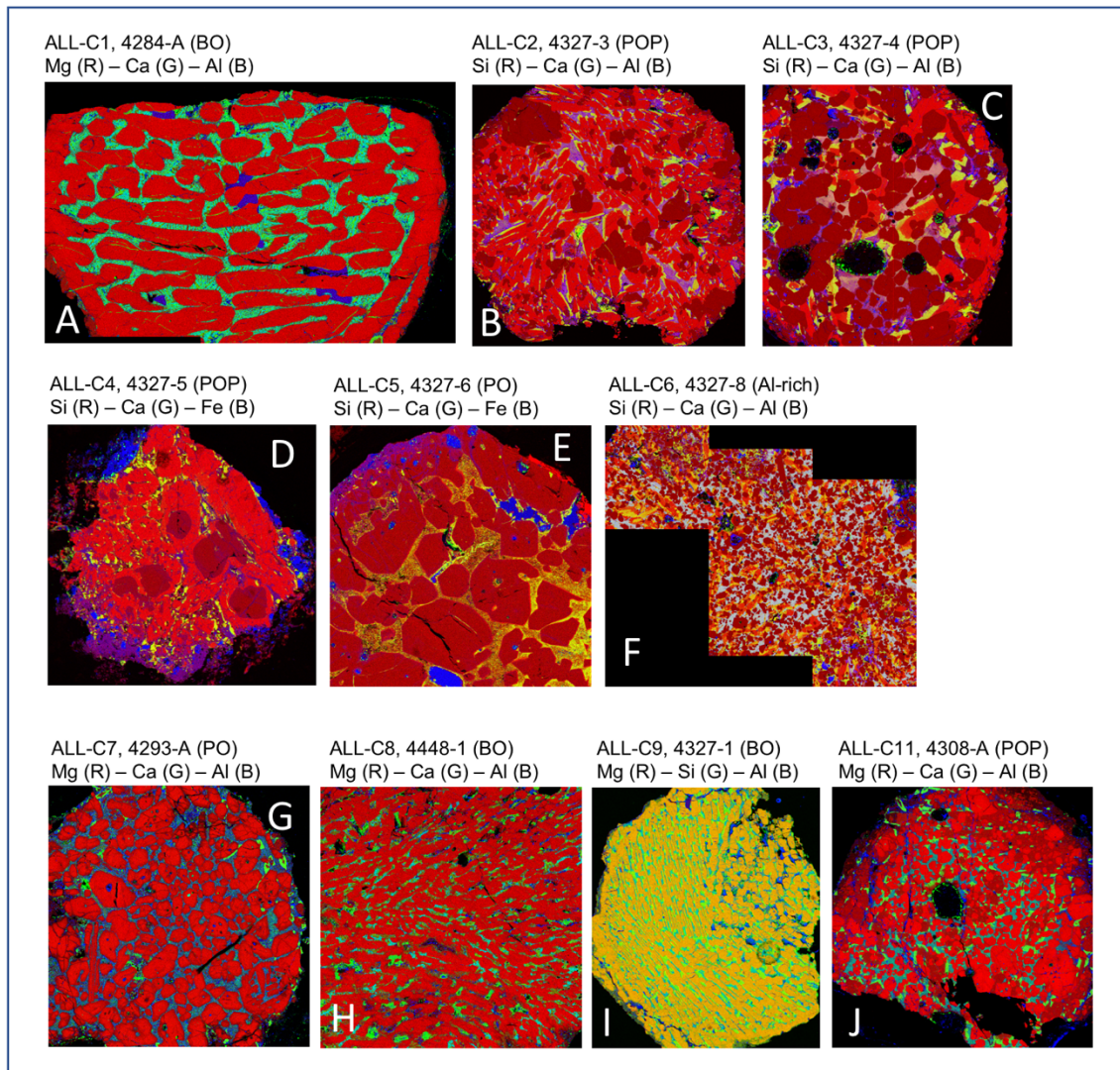


Fig. S4. Combined X-ray elemental maps of selected Karoonda chondrules with Mg (red)- Ca (green)- Al (blue). Olivine is shown as red, high Ca-pyroxene as green, plagioclase as greenish blue. In KR-C3 (A), hercynite-rich spinel appears as darker blue.

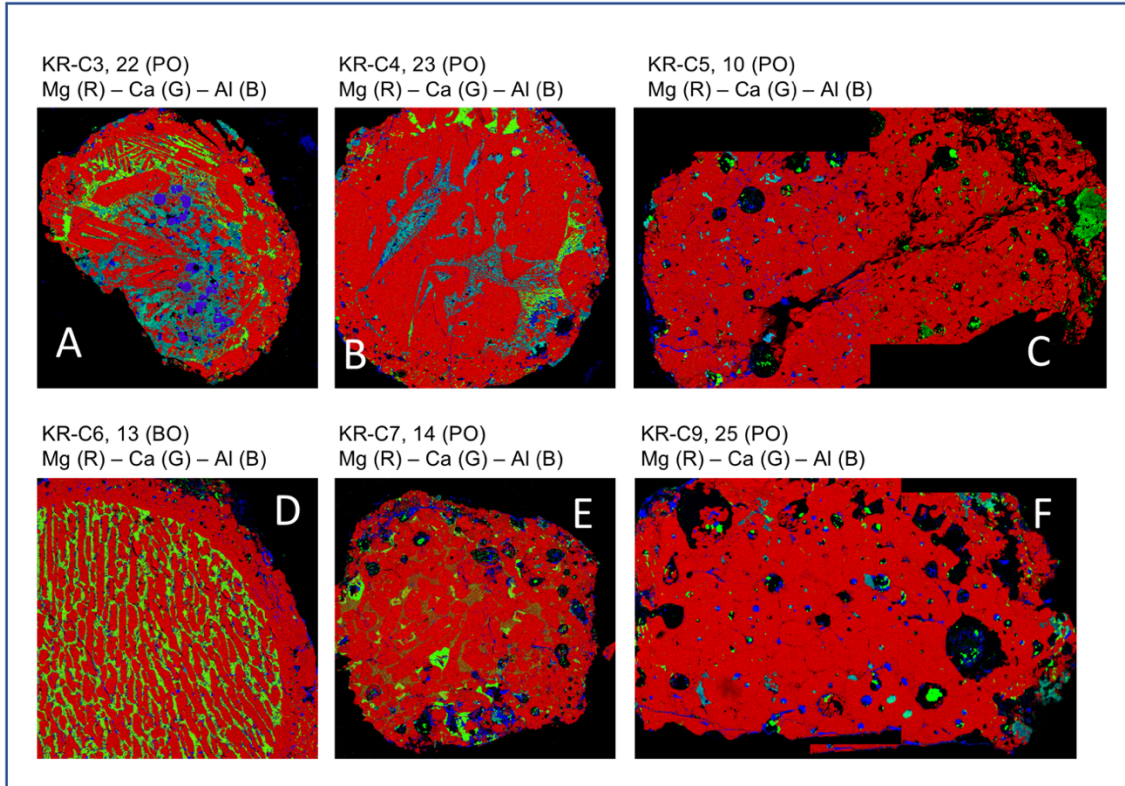
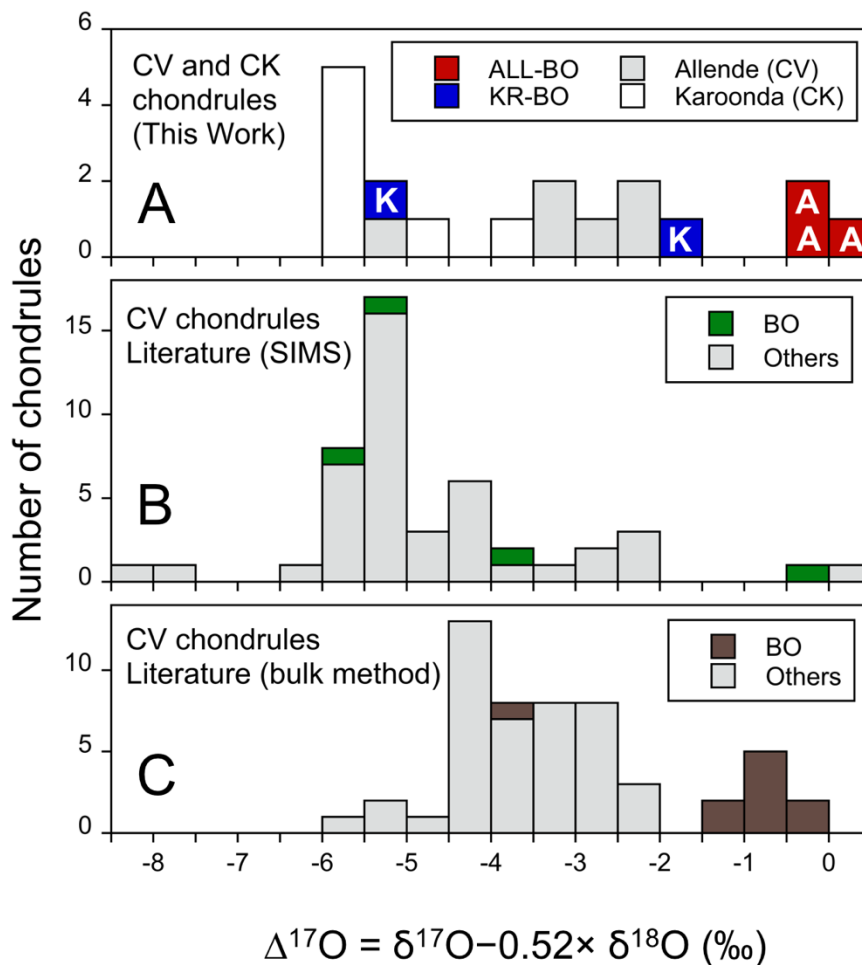


Fig. S5. Histogram of $\Delta^{17}\text{O}$ of individual chondrules. Chondrules in CV chondrites from this study (A), literature with SIMS analyses (B), and literature with bulk method (C). Literature data are from (13, 17, 44-45, 48). Literature SIMS data do not show systematic differences between BO chondrules and other chondrules. However, literature data using bulk method show significant numbers of BO chondrules at the highest $\Delta^{17}\text{O}$ values, which are similar to the three BO chondrules in Allende that were analyzed in this study. Literature SIMS data are obtained mainly from average ~ 1 mm size chondrules, while literature bulk method data include those with larger than mean CV chondrite chondrule diameters. While contribution from altered mesostasis would increase $\Delta^{17}\text{O}$ of chondrules using bulk methods, scarcely of $\sim \Delta^{17}\text{O} = -5\text{‰}$ chondrules among data using bulk methods suggest that there could be systematic difference between population of chondrules depend on the sizes of chondrules.



Dataset S1. Ti-Cr-O isotopic composition of bulk meteorites.

Uploaded as excel file.

Dataset S2. Petrology, mineral chemistry, and Ti-Cr-O isotopic composition of individual chondrules.

Uploaded as excel file.

Dataset S3. Cr isotopic composition of individual chondrules.

Uploaded as excel file.

Dataset S4. Oxygen three-isotope analyses of Allende chondrules using SIMS.

Uploaded as excel file.

Dataset S5. Oxygen three-isotope analyses of Karoonda chondrules using SIMS.

Uploaded as excel file.

Dataset S6. Representative mineral compositions in Allende and Karoonda chondrules.

Uploaded as excel file.

References

77. T. Noguchi, Petrology and mineralogy of CK chondrites: implications for the metamorphism of the CK chondrite parent body. *Proc. NIPR Symp. Antarct. Meteorites.* **6**, 204–233 (1993).
78. R. H. Jones, Petrographic constraints on the diversity of chondrule reservoirs in the protoplanetary disk. *Meteor. Planet. Sci.* **47**, 1176–1190 (2012).